Optics Letters

# DFB laser array based on four phase-shifted sampled Bragg gratings with precise wavelength control

Yiming Sun,[1,*] Bocheng Yuan,[1] Xiao Sun,[1] Song Liang,[2] Yongguang Huang,[2] Ruikang Zhang,[2] Shengwei Ye,[1] Yizhe Fan,[1] Weiqing Cheng,[1] John H. Marsh,[1] and Lianping Hou[1]

[1]James Watt School of Engineering, University of Glasgow, Glasgow G12 8QQ, UK
[2]Institute of Semiconductors, Chinese Academy of Sciences, No. A35, East Qinghua Road, Haidian District, Beijing 100083, China
*Corresponding author: 2465522S@student.gla.ac.uk

Received 16 September 2022; revised 3 November 2022; accepted 4 November 2022; posted 4 November 2022; published 29 November 2022

**A four-laser array based on sampled Bragg grating distributed feedback (DFB) lasers in which each sampled period contains four phase-shift sections is proposed, fabricated, and experimentally demonstrated. The wavelength spacing between adjacent lasers is accurately controlled to 0.8 nm ± 0.026 nm and the lasers have single mode suppression ratios larger than 50 dB. Using an integrated semiconductor optical amplifier, the output power can reach 33 mW and the optical linewidth of the DFB lasers can be as narrow as 64 kHz. This laser array uses a ridge waveguide with sidewall gratings and needs only one metalorganic vapor-phase epitaxy (MOVPE) step and one III-V material etching process, simplifying the whole device fabrication process, and meeting the requirements of dense wavelength division multiplexing systems.**



https://doi.org/10.1364/OL.475909

To meet the requirements of the massive growth in Internet traffic, integrated dense wavelength division multiplexing (DWDM) systems have been proposed due to their low power consumption, compact size, and high reliability [1]. A multi-wavelength array of distributed feedback (DFB) lasers with precise channel spacing is considered to be a key component for the DWDM source [2]. For arrays of single longitudinal mode (SLM) lasers, one of the most important features is the accurate control of each laser's lasing wavelength, which must meet the requirement of the ITU-T wavelength spacing standard. Therefore, the grating period of each laser needs to be individually controlled with very high accuracy. In DWDM systems, the period difference between two neighboring DFB lasers is quite small; for example, when the effective index ($n_{eff}$) is 3.2, the standard wavelength spacing of 0.8 nm corresponds to a difference of only 0.125 nm in the grating period, which is even beyond the typical resolution limit of 0.5 nm of electron beam lithography (EBL). Therefore, thermal tuning of each laser in the array is usually used to control the lasing wavelength which may increase the cost of the fabrication and decrease the product yield. Meanwhile, additional problems such as decreased quantum efficiency of the lasers and spatial hole burning (SHB) effects can occur in the device.

Reconstruction equivalent-chirp (REC) technology has contributed significantly to reducing the difficulty of achieving high-precision wavelength control in laser arrays [3]. Based on REC technology, a seed Bragg grating of constant period is used across the entire array, but the seed grating is sampled with the dimensions of the sampling period determining the wavelength of operation of each laser. REC designs usually use conventional sampled Bragg gratings (C-SBG) where 50% of each period is a grating and the remaining 50% has no grating [4]. However, C-SBGs only have an effective grating coupling coefficient $\kappa$ equal to $1/\pi$ of that of a uniform grating [4]. In addition, the reflection of the $0^{th}$ channel is also present and can adversely affect the performance of a C-SBG laser. In [5], a sidewall DFB laser array based on a two phase-shifted sampled Bragg grating (2PS-SBG) was reported with an effective $\kappa$ equal to $2/\pi$ of that of a uniform grating and precise channel spacing of 0.8 nm.

In this Letter, a four-wavelength sidewall DFB array with a wavelength spacing of 0.8 nm is reported using, for the first time, four phase-shifted sampled Bragg grating (4PS-SBG) structures in which each period has four phase-shifted sections. Compared with buried C-SBG DFB laser arrays which need complicated epilayer etching and regrowth [4], sidewall grating DFB lasers need only one metalorganic vapor-phase epitaxy (MOVPE) step and one III-V material etching process, simplifying the whole device fabrication process. The effective $\kappa$ value of the $+1^{st}$ channel is significantly enhanced in the 4PS-SBG structure compared to a C-SBG in [4] and 2PS-SBG in [5], and is equal to 0.9 of that of a uniform grating. The output power from the semiconductor optical amplifier (SOA) facet can reach 33 mW with a narrow linewidth.

Figures 1(a) and 1(b) show schematics of the C-SBG and the 4PS-SBG, respectively. For the C-SBG, half of the sampling period has no grating, resulting in the coupling efficiency $\kappa$ in the $\pm 1^{st}$ channel decreasing to only $1/\pi$ times that of a uniform

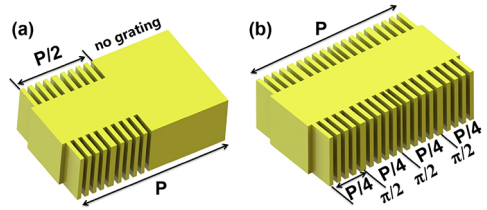


**Fig. 1.** Grating structures of (a) C-SBG, (b) 4PS-SBG. $P$ is the sampling period.

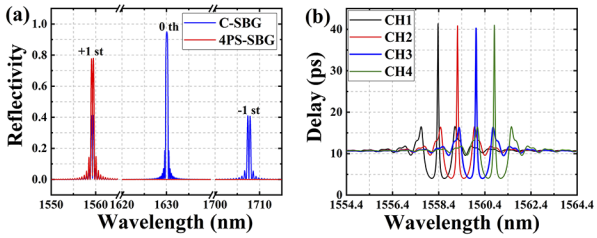


**Fig. 2.** (a) Calculated reflection spectra of 4PS-SBG with a π phase-shift in the center of the cavity (red curve) compared with that of the C-SBG (blue curve). (b) Time-delay spectrum under different sampling periods.

grating. For the 4PS-SBG, the grating in each sampling period is evenly divided into four sections with each adjacent grating section subjected to a π/2 phase-shift. This structure simultaneously enhances the effective κ of the $+1^{st}$ channel to 0.90 times that of a uniform Bragg grating and eliminates the $0^{th}$ channel reflection [6].

Using the transfer matrix method (TMM), we calculated the reflection and time-delay spectra of the 4PS-SBG structure, which are shown in Fig. 2. Compared with the C-SBG structure, in the 4PS-SBG structure, the $0^{th}$ channel disappears and the $+1^{st}$ channel is significantly enhanced, as shown in Fig. 2(a). When a π phase-shift of the seed grating period $\Lambda_0$ is inserted into the middle of the cavity, a resonance peak that represents the lasing mode appears in the center of the stop band of the $+1^{st}$ channel. The wavelength of the $+1^{st}$ channel can be expressed as

$$\lambda_{+1} = 2n_{eff} \cdot \frac{P\Lambda_0}{P + \Lambda_0}, \tag{1}$$

where $n_{eff}$ is the effective refractive index of the ridge waveguide, $P$ is the sampling period, and $\Lambda_0$ is the seed grating period as described above. For the designed and calculated values, $\Lambda_0$ is 257 nm, which locates the $0^{th}$ channel at 1630 nm; the $+1^{st}$ channel, used as the output channel, is located at the gain peak of the multiple quantum well (MQW) material, which is around 1560 nm; $n_{eff}$ is 3.19 and the dispersion coefficient is −0.00021/nm. Based on the above data and considering the EBL resolution limit to be 0.5 nm, we designed a 4 SLM laser array (CH1 to CH4). The $P$ for CH1 to CH4 was changed from 4.867 μm to 5.037 μm. The detailed designed values of the $P$ and the corresponding lasing wavelengths are shown in Table 1. The time-delay spectrum under different $P$ is shown in Fig. 2(b). From Table 1 and Fig. 2(b), a difference in the sampling period of 56 nm results in lasing wavelengths being separated by 0.8 nm. This sampling period difference is much larger than that of the EBL's typical resolution of 0.5 nm and so is straightforward to fabricate.

**Table 1. Sampling Period $P$ Values for Different Wavelengths**

| Channel No. | Sampling Period $P$/μm | Wavelength/nm |
|---|---|---|
| CH1 | 4.867 | 1558.4 |
| CH2 | 4.923 | 1559.2 |
| CH3 | 4.979 | 1560.0 |
| CH4 | 5.037 | 1560.8 |

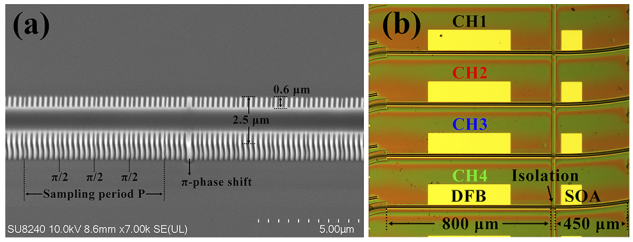


**Fig. 3.** (a) SEM picture of 4PS-SBG sidewall grating with ridge waveguide width of 2.5 μm and a recess depth of 0.6 μm. (b) Optical microscopy picture of the fabricated four channel 4PS-SBG structure DFB laser array.

The epitaxial structure used for the devices was based on the AlGaInAs/InP material system and contains five quantum wells (QWs) and six quantum barriers (QBs). The detailed epilayer structure is referenced in [5] and the device fabrication process is similar to that described in [7].

Figure 3(a) shows a scanning electron microscopy (SEM) picture of a 4PS-SBG sidewall grating structure with a ridge waveguide width of 2.5 μm and a grating recess depth of 0.6 μm on each side of the ridge. Each sampling period contains four sections, and there is a π/2 phase difference between adjacent sections. Meanwhile, a π phase shift of the seed grating period $\Lambda_0$ was inserted into the center of the cavity of the 800-μm-long DFB laser to ensure SLM operation of the device, as shown in Fig. 2(a).

Figure 3(b) shows an optical microscopy picture of the fabricated 4PS-SBG DFB laser array. Each device consists of three sections: two curved waveguides located on the front and rear sides, respectively, to reduce facet reflections, with the 800-μm-long DFB section in the middle. The front 450-μm-long curved waveguide also includes an SOA with a radius of 1810 μm, making a tilt angle of 10° at the output facet resulting in an intensity reflectivity of approximately $10^{-4}$ at 1550 nm. The isolation gap between DFB and SOA sections is 20 μm wide with the heavily doped 250-nm $p^+$ cap layer removed to give an electrical isolation of approximately 15 kΩ. On the back side of the DFB laser diode, a 125-μm-long waveguide with a radius of 233.3 μm and a tilt angle of 32° was applied. In the final stage of fabrication, the sample was cleaved into individual laser bars and was mounted epilayer-up on a copper heat sink on a Peltier cooler. The heat sink temperature was set at 20°C and the devices were tested under CW conditions.

Figure 4 shows typical output power versus DFB current ($I_{DFB}$) ($P$–$I_{DFB}$) characteristics for CH1 under different SOA currents ($I_{SOA}$). The threshold current of the DFB laser is 37 mA. When fixing $I_{DFB}$ and increasing $I_{SOA}$, the output power from the SOA side is increased. When $I_{DFB}$ = 206 mA and $I_{SOA}$ = 120 mA, the output power reaches its maximum value of 33 mW. For all the $P$–$I_{DFB}$ curves, a relatively larger slope efficiency is observed between 37 mA and 50 mA. This is because the SOA has a

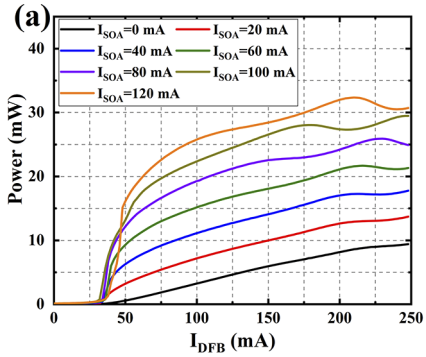


**Fig. 4.** Typical $P$–$I_{DFB}$ curves under different $I_{SOA}$ measured from the SOA side.

larger amplification for the relatively lower optical power from the DFB part. As $I_{DFB} > 50$ mA, the optical power from the DFB part becomes larger, resulting in a decrease in SOA amplification and a relatively lower slope efficiency [8]. As for $I_{DFB} > 175$ mA, several kinks observed in all the $P$–$I$ curves' characteristics indicate that the DFB laser is disturbed by the amplified back-reflection from the SOA facet. To compare the $\kappa$ of a uniform grating and 4PS structures, DFB lasers with a uniform grating (other than a $\pi$-phase shift section inserted at the center of the DFB laser cavity) and the 4PS structure were fabricated on the same wafer. The measured spectra with $I_{DFB} = 34$ mA and $I_{SOA} = 30$ mA are shown in Fig. 5. From coupled mode theory, the $\kappa$ can be calculated from $\Delta\lambda_s$ and $\lambda_B$ using the following formula [9]:

$$\kappa = n_{eff} \cdot \frac{\Delta\lambda_s}{\lambda_B^2}, \tag{2}$$

where $n_{eff}$ is the effective index; $\Delta\lambda_s$ is the stop band width; $\lambda_B$ is the Bragg wavelength of the grating. Figures 5(a) and 5(b) show the measured optical spectrum for 800-μm-long DFB lasers with a uniform grating and 4PS-SBG, respectively. For the uniform grating, the stop band width $\Delta\lambda_s$ is 1.378 nm and the Bragg wavelength $\lambda_B$ is 1550.9 nm. For 4PS-SBG, the stop band width $\Delta\lambda_s$ is approximately 1.15 nm, and the Bragg wavelength $\lambda_B$ is approximately 1558.3 nm. Therefore, the $\kappa$ values of the uniform grating and 4PS-SBG devices are calculated as 18.28 $cm^{-1}$ and 15.12 $cm^{-1}$, respectively. The ratio of the effective $\kappa$ of the 4PS-SBG to that of the uniform grating is approximately 0.83, lower than the theoretical value of 0.9, which is probably due to the reactive ion etching (RIE) lag effect during the sidewall grating fabrication [10]. RIE lag is more obvious during the fabrication of the 4PS device because the 4PS grating patterns contain many narrow recesses at the $\pi/2$ phase shift position, as shown

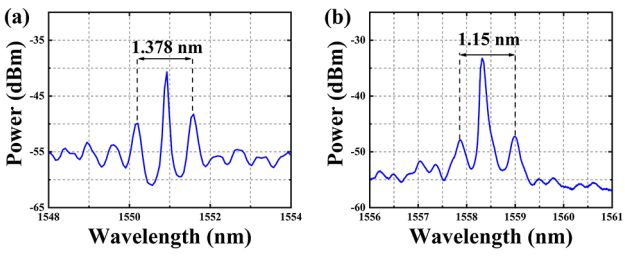


**Fig. 5.** Optical spectrum at threshold current of (a) uniform grating with a $\pi$-phase shift section inserted at the center of the DFB laser cavity and (b) 4PS-SBG structure.

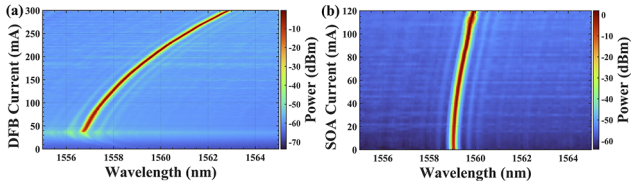


**Fig. 6.** (a) 2D optical spectra versus $I_{DFB}$ of CH1 with $I_{SOA} = 30$ mA. (b) 2D optical spectra versus $I_{SOA}$ with $I_{DFB} = 180$ mA.

in Fig. 3(a). However, the results still show that the value of $\kappa$ is significantly enhanced using the 4PS-SBG structure.

Figure 6(a) shows a two-dimensional (2D) optical spectrum versus $I_{DFB}$ (0–300 mA) with $I_{SOA} = 30$ mA for CH1. Very stable SLM operation is observed from the threshold current (37 mA) up to 300 mA, with no mode-hopping. The average current induced wavelength redshift coefficient is approximately 0.023 nm/mA, which is much smaller than that of an Fabry–Perot laser and allows for fine-tuning of wavelengths across the DWDM laser array. Figure 6(b) shows the 2D optical spectrum versus $I_{SOA}$ (0–120 mA) when $I_{DFB} = 180$ mA. Again, stable SLM operation is observed, and the current-induced redshift is approximately 0.0075 nm/mA, which means varying the SOA current has a negligible effect on the DFB lasing wavelength while enabling the SOA to be used to boost the output power.

Figure 7(a) shows the optical spectra for each channel with $I_{SOA} = 30$ mA and $I_{DFB} = 180$ mA. The spectrum was measured using an optical spectrum analyzer (OSA) with a resolution bandwidth of 0.06 nm. The lasing wavelengths are 1559.64 nm, 1560.44 nm, 1561.22 nm, and 1561.96 nm from CH1 to CH4. These measured lasing wavelengths are nearly the same as the designed ones (shown in Table 1).

Figure 7(b) shows the corresponding linear fit to the lasing wavelengths of the four channels, and the slope of the line is 0.774 nm, with an error of 0.026 nm compared with the designed wavelength spacing of 0.8 nm. The value of this error is less than the resolution of the OSA, which demonstrates the excellent wavelength precision that can be achieved by the 4PS-SBG structure.

The SMSR of the four devices versus $I_{DFB}$ is shown in Fig. 8. The SMSRs of all four channels are larger than 50 dB when $I_{DFB} > 100$ mA and the maximum SMSR value can reach 55 dB when $I_{DFB} = 250$ mA.

The linewidth of the fabricated 4PS device was measured using the delayed self-heterodyne method with a 4.4-km single-mode fiber and an 80-MHz acoustic-optic modulator [11]. During the test, the resolution of the electrical signal analyzer (ESA) was kept at 20 kHz, and the measured radio frequency (RF) spectra were fitted to Lorentz and Voigt profiles to calculate

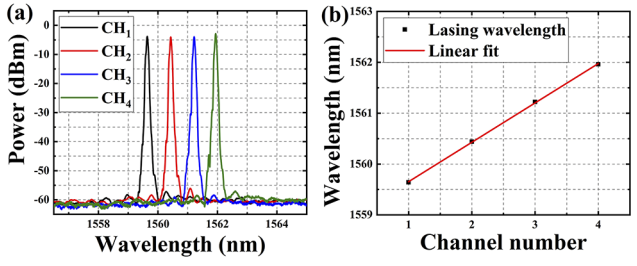


**Fig. 7.** (a) Measured optical spectrum of the devices for different periods, $P$, when $I_{DFB} = 180$ mA, $I_{SOA} = 30$ mA. (b) Lasing wavelengths and linear fit to the four points.

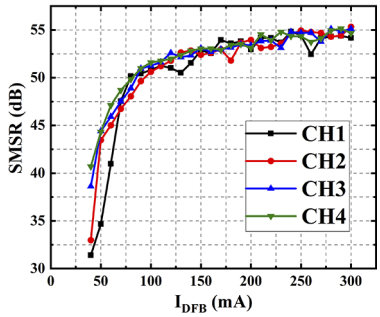


**Fig. 8.** SMSRs of four lasers versus $I_{DFB}$ when $I_{SOA}$ is 30 mA.

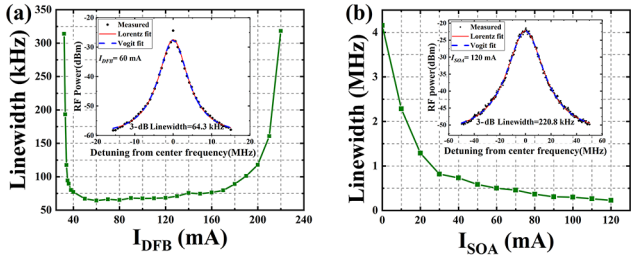


**Fig. 9.** (a) Optical linewidth versus $I_{DFB}$ without SOA. Inset shows the measured RF spectrum of the beat note signal (black dots) and its Lorentz (red line) and Voigt profile (blue dash line) fitting at $I_{DFB} = 60$ mA. (b) Optical linewidth versus the $I_{SOA}$ with $I_{DFB} = 180$ mA. Inset shows the measured RF spectrum of the beat note signal and its Lorentz (red line) and Voigt profile (blue dash line) fitting at $I_{SOA} = 120$ mA.

the −3-dB linewidth of the DFB laser. Figure 9(a) shows the −3-dB linewidth as a function of $I_{DFB}$ measured from the 4PS-SBG DFB laser's cleaved straight output facet after removing the SOA section. The DFB laser maintained a stable SLM operation from threshold current to 300 mA without mode-hopping. The measured RF spectrum of the beat note signal (black dots) shown in the inset of Fig. 9(a) was fitted to a Lorentz profile (red line) and a Voigt profile (blue dash line). Here, we note the trend that the linewidth reduces rapidly when $I_{DFB}$ is increased from 32 mA to 60 mA. After that, the value of the linewidth remains stable at approximately 70 kHz from $I_{DFB} = 60$ to 140 mA (the slight increase of linewidth may be due to an approximately 16°C temperature rise with drive current), with the narrowest linewidth of 64.3 kHz observed at $I_{DFB} = 60$ mA. This narrow optical linewidth may be due to the long DFB cavity length of 800 μm and the relatively high $\kappa L$ value of 1.21 [12]. As the $I_{DFB}$ continues to increase, the value of the linewidth increases, which may be due to the SHB effect at high injection currents. Figure 9(b) shows the measured optical linewidth of a DFB laser integrated with SOA as a function of $I_{SOA}$ with $I_{DFB} = 180$ mA. The optical linewidth at $I_{SOA} = 0$ mA is 4.16 MHz. Compared to the linewidth of DFB lasers without SOAs, the SOA adds significant noise, which results in the linewidth increasing. According to [13], if the reflection from the SOA is less than $1 \times 10^{-5}$, the optical linewidth broadens with increasing $I_{SOA}$, and the influence of amplified spontaneous emission (ASE) on the optical linewidth is slight. Since the reflection coefficient of the uncoated 10° angled SOA output facet is approximately $1 \times 10^{-4}$, the portion of the output light re-injected back into the DFB cavity will result in a reduction of the linewidth as $I_{SOA}$ increases owing to increased optical feedback and frequency coherence [14]. The inset shows the measured RF spectrum of the beat note signal (black dots) with good fits to a Lorentz profile (red line) and a Voigt profile (blue dash line) at $I_{SOA} = 120$ mA, where the linewidth is 220.8 kHz. By using additional anti-reflection (AR) coatings on the SOA facet with less than $1 \times 10^{-5}$ reflection, the influence of external feedback into the SOA will be less and a relatively constant optical linewidth from the SOA facet is expected [12,13].

In conclusion, an SLM laser array based on the 4PS-SBG structure is proposed and experimentally demonstrated for the first time, to the best of our knowledge. Measurement results show that the 4PS-SBG structure gives precise control over the individual DFB laser lasing wavelengths accompanied by a high coupling coefficient. SML operation was maintained over a wide range of drive currents of both the DFB and SOA, and a 55-dB SMSR with an output power of approximately 33 mW was achieved. Narrow linewidths of 64.3 kHz from a DFB laser and 220.8 kHz from a DFB laser plus SOA were obtained. The sidewall grating 4PS-SBG DFB laser array needs only one MOVPE step and one dry etch of the III-V material, simplifying the whole device fabrication process, which is a highly desirable feature for DWDM sources in price sensitive applications such as passive optical networks (PONs).

**Funding.** Engineering and Physical Sciences Research Council (EP/R042578/1); Chinese Ministry of Education Collaborative Project (B17023).

**Acknowledgments.** We would like to acknowledge the staff of the James Watt Nanofabrication Centre at the University of Glasgow for their help in fabricating the devices.

**Disclosures.** The authors declare no conflict of interest.

**Data availability.** Data underlying the results presented in this paper are not publicly available at this time but may be obtained from the authors upon reasonable request.

## REFERENCES

1. H. Debrégeas-Sillard and C. Kazmierski, C. R. Phys. **9**, 1055 (2008).
2. O. K. Kwon, Y. A. Leem, Y. T. Han, C. W. Lee, K. S. Kim, and S. H. Oh, Opt. Express **22**, 9073 (2014).
3. Y. Dai, X. Chen, L. Xia, Y. Zhang, and S. Xie, Opt. Lett. **29**, 1333 (2004).
4. Y. Shi, X. Chen, Y. Zhou, S. Li, L. Lu, R. Liu, and Y. Feng, Opt. Lett. **37**, 3315 (2012).
5. S. Tang, L. Hou, X. Chen, and J. H. Marsh, Opt. Lett. **42**, 1800 (2017).
6. J. Li, Y. Cheng, Z. Yin, L. Jia, X. Chen, S. Liu, S. Li, and Y. Lu, IEEE Photonics Technol. Lett. **21**, 1639 (2009).
7. L. Hou, M. Haji, J. Akbar, J. H. Marsh, and A. C. Bryce, IEEE J. Quantum Electron. **48**, 137 (2012).
8. P. W. Juodawlkis, J. J. Plant, W. Loh, L. J. Missaggia, K. E. Jensen, and F. J. O'Donnell, IEEE Photonics Technol. Lett. **21**, 1208 (2009).
9. M. Razeghi, R. Blondeau, M. Krakowski, J. C. Bouley, M. Papuchon, B. Cremoux, and J. Duchemin, IEEE J. Quantum Electron. **21**, 507 (1985).
10. S. Guilet, S. Bouchoule, C. Jany, C. Corr, and P. Chabert, in *2006 International Conference on Indium Phosphide and Related Materials Conference Proceedings* (IEEE, 2006), 262–265.
11. T. N. Huynh, L. Nguyen, and L. P. Barry, IEEE Photonics Technol. Lett. **24**, 249 (2012).
12. H. Ishii, K. Kasaya, and H. Oohashi, IEEE J. Sel. Top. Quantum Electron. **15**, 514 (2009).
13. T. Kimoto, T. Kurobe, K. Muranushi, T. Mukaihara, and A. Kasukawa, IEEE J. Sel. Top. Quantum Electron. **11**, 919 (2005).
14. H. G. Zhang, N. H. Zhu, J. W. Man, J. H. Ke, B. H. Zhang, W. Han, W. Chen, H. Q. Yuan, X. Wang, L. Xie, L. J. Zhao, and W. Wang, IEEE Photonics Technol. Lett. **21**, 1045 (2009).